Please cite this article in press as: Rhim et al., Stromal Elements Act to Restrain, Rather Than Support, Pancreatic Ductal Adenocarcinoma, Cancer Cell (2014), http://dx.doi.org/10.1016/j.ccr.2014.04.021

Cancer Cell
Article

Stromal Elements Act to Restrain, Rather Than Support, Pancreatic Ductal Adenocarcinoma

Andrew D. Rhim,[1,2,8] Paul E. Oberstein,[3,8] Dafydd H. Thomas,[4,5,8] Emily T. Mirek,[2] Carmine F. Palermo,[4,5] Stephen A. Sastra,[4,5] Erin N. Dekleva,[2] Tyler Saunders,[6] Claudia P. Becerra,[5] Ian W. Tattersall,[5] C. Benedikt Westphalen,[4] Jan Kitajewski,[5] Maite G. Fernandez-Barrena,[7] Martin E. Fernandez-Zapico,[7] Christine Iacobuzio-Donahue,[6] Kenneth P. Olive,[4,5,*] and Ben Z. Stanger[2,*]

[1]Division of Gastroenterology, Department of Internal Medicine and Comprehensive Cancer Center, University of Michigan Medical School, Ann Arbor, MI 48109, USA
[2]Gastroenterology Division, Department of Medicine and Abramson Family Cancer Research Institute, Perelman School of Medicine, University of Pennsylvania, Philadelphia, PA 19104, USA
[3]Division of Hematology and Oncology
[4]Division of Digestive and Liver Diseases in the Department of Medicine
[5]Department of Pathology and Cell Biology
Herbert Irving Comprehensive Cancer Center, Columbia University Medical Center, New York, NY 10032, USA
[6]Sol Goldman Pancreatic Cancer Research Center and Department of Pathology, Johns Hopkins University, Baltimore, MD 21287, USA
[7]Schulze Center for Novel Therapeutics, Mayo Clinic, Rochester, MN 55905, USA
[8]Co-first author
*Correspondence: kenolive@columbia.edu (K.P.O.), bstanger@exchange.upenn.edu (B.Z.S.)
http://dx.doi.org/10.1016/j.ccr.2014.04.021

SUMMARY

Sonic hedgehog (Shh), a soluble ligand overexpressed by neoplastic cells in pancreatic ductal adenocarcinoma (PDAC), drives formation of a fibroblast-rich desmoplastic stroma. To better understand its role in malignant progression, we deleted Shh in a well-defined mouse model of PDAC. As predicted, Shh-deficient tumors had reduced stromal content. Surprisingly, such tumors were more aggressive and exhibited undifferentiated histology, increased vascularity, and heightened proliferation—features that were fully recapitulated in control mice treated with a Smoothened inhibitor. Furthermore, administration of VEGFR blocking antibody selectively improved survival of Shh-deficient tumors, indicating that Hedgehog-driven stroma suppresses tumor growth in part by restraining tumor angiogenesis. Together, these data demonstrate that some components of the tumor stroma can act to restrain tumor growth.

INTRODUCTION

Pancreatic ductal adenocarcinoma (PDAC) is notable for its profuse desmoplastic stroma comprised of activated fibroblasts, leukocytes, and extracellular matrix (Olive et al., 2009; Theunissen and de Sauvage, 2009). Studies utilizing in vitro assays and transplantation models have concluded that various stromal elements can enhance cancer cell proliferation and invasion (Hwang et al., 2008; Ikenaga et al., 2010; Lonardo et al., 2012; Vonlaufen et al., 2008; Xu et al., 2010). Various stromal cells can also contribute to immune suppression, further supporting tumor survival and growth. Together, these observations have led to the paradigm that tumor stroma functions to support and promote the growth of cancer (Hanahan and Weinberg, 2011). Based on this paradigm, the concept of "antistromal" therapy has emerged as a

Significance

Numerous therapies are being developed based on the premise that tumor stroma functions to promote cancer growth and invasion while simultaneously limiting the delivery of chemotherapy. Here, we demonstrate that depletion of stromal cells from pancreatic tumors—through genetic or pharmacological targeting of the Hh pathway—results in a poorly differentiated histology, increased vascularity and proliferation, and reduced survival. The study thus provides insight into the failure of Smoothened inhibitors, an antistromal therapy, in pancreatic cancer clinical trials. Moreover, we report that Hh-deficient tumors exhibit an increased sensitivity to VEGFR inhibition. Because poorly differentiated human pancreatic tumors are well-vascularized, in contrast to most pancreatic cancers, our results suggest that this patient subset may be susceptible to angiogenesis inhibitors.

Please cite this article in press as: Rhim et al., Stromal Elements Act to Restrain, Rather Than Support, Pancreatic Ductal Adenocarcinoma, Cancer Cell (2014), http://dx.doi.org/10.1016/j.ccr.2014.04.021

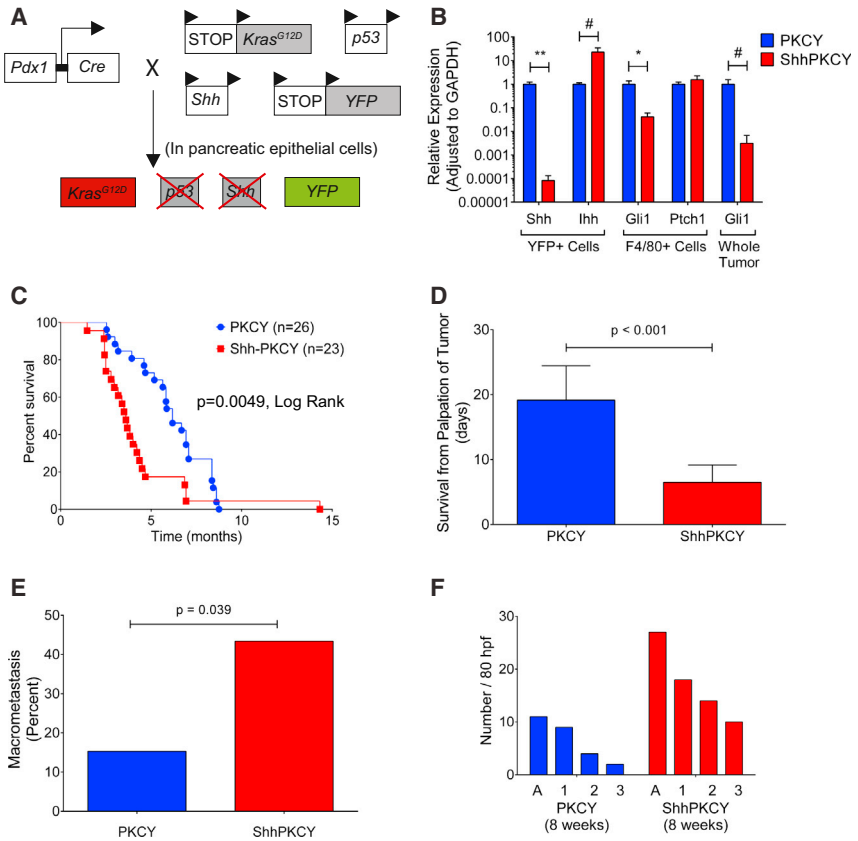

Figure 1. Sonic Hedgehog Behaves as a Tumor Suppressor in a Genetically Engineered Mouse Model of PDAC

(A) Schematic of the ShhPKCY mouse model used in this study, which employs the *Kras*^{G12D} (K), *Pdx1-Cre* (C), *p53* (P), *Rosa*^{YFP} (Y), and *Shh* alleles. Cre-mediated deletion results in simultaneous activation of *Kras*, deletion of one allele of *p53*, and both alleles of *Shh* and recombination of the *YFP* lineage label.

(B) Confirmation of Shh knockdown in ShhPKCY animals. Quantitative PCR analysis of Hedgehog signaling components in YFP$^+$ sorted pancreatic epithelial derived cells and F4/80$^+$ cells from tumors as well as whole tumor derived from PKCY (blue) and ShhPKCY (red) mice (n = 5 for each group; bars represent means ± SD).

(C) Kaplan-Meier survival analysis for PKCY (n = 26) and ShhPKCY mice (n = 23). $p < 0.005$ by Mantel-Cox (log rank) test.

(D) Survival of mice from first clinical palpation of tumor. Presence of tumor was confirmed by ultrasound. Bars represent means ± SD; $p < 0.001$.

(E) Fraction of mice with any macrometastatic lesion by visual inspection at the time of tissue harvest by genotype (n = 26 and 23 for PKCY and ShhPKCY mice, respectively). $p = 0.039$.

(F) Quantitation of acinar to ductal metaplasia (bar A) and PanIN lesions by grade (bars 1–3) in 8-week-old PKCY and ShhPKCY mice. Eighty nonoverlapping high powered fields in which pancreas tissue covered at least 90% of the entire field were analyzed (n = 3 for each group).

Data are presented as the aggregate number of ADMs and PanINs (by grade) for each genotype. #, $p < 0.05$; *, $p < 0.01$; **, $p < 0.001$ by two-tailed Student's t test. See also Figure S1.

promising, albeit unproven, therapeutic approach (Engels et al., 2012).

The Hedgehog (Hh) signaling pathway contributes to stromal desmoplasia in multiple solid tumor systems. Although normally absent in the adult pancreas, this developmental morphogen pathway is reactivated during inflammation and neoplasia. Both sonic hedgehog (Shh) ligand and downstream signaling are induced de novo in preneoplastic lesions and increase significantly during PDAC progression as the stromal compartment enlarges (Thayer et al., 2003). Although ectopic activation of Hh signaling within pancreatic epithelial cells can accelerate tumorigenesis (Mao et al., 2006; Morton et al., 2007; Pasca di Magliano et al., 2006), deletion of the Hh signaling mediator Smoothened (Smo) from the epithelium has no impact on PDAC progression (Nolan-Stevaux et al., 2009). Hence, canonical Hh signaling in PDAC is likely to occur in a paracrine fashion, whereby Shh ligand secreted from epithelial cells activates Smo-dependent downstream signaling in adjacent stromal cells, promoting desmoplasia (Bailey et al., 2008; Tian et al., 2009). The notion that Hh-dependent tumor stroma facilitates tumorigenesis is supported by the finding that inhibiting Hh signaling retards pancreatic tumor growth and metastasis in transplantation models (Bailey et al., 2008; Feldmann et al., 2008a, 2008b) and through our own study of the effects of acute inhibition of Smo in genetically engineered mouse models (Olive et al., 2009). In this study, we sought to interrogate the role of the tumor stroma by using both genetic deletion and long-term pharmacologic inhibition to eliminate stroma-promoting Hh signaling.

RESULTS

Shh Loss Accelerates PDAC Progression

To explore the role of paracrine Hh signaling in an autochthonous mouse model of PDAC, we conditionally deleted *Shh*, the predominant Hh ligand expressed in the diseased pancreas, by breeding Shh^{fl} alleles into the *Pdx1-Cre;Kras*$^{LSL\text{-}G12D/+}$*;p53*$^{fl/+}$*;Rosa26*$^{LSL\text{-}YFP/+}$ (PKCY) model (Rhim et al., 2012). Because *Pdx1-Cre* mediates recombination exclusively in the epithelial cells of the pancreas (Rhim et al., 2012), this combination of alleles results in the simultaneous activation of mutant *Kras* and deletion of *Shh* and *p53* within this tissue compartment (Figure 1A). *Shh* deletion had no effect on pancreatic development (Figure S1A available online), and the resulting *Shh*$^{fl/fl}$*;Pdx1-Cre;Kras*$^{LSL\text{-}G12D/+}$*;p53*$^{fl/+}$*;Rosa26*$^{LSL\text{-}YFP}$ (ShhPKCY) mice were born at expected Mendelian ratios and were phenotypically normal at birth.

To confirm the deletion of *Shh* in the pancreatic epithelial compartment, we performed transcriptional analysis on FACS-sorted yellow fluorescent protein (YFP$^+$) cells from 10- to 16-week-old PKCY and ShhPKCY mice (Rhim et al., 2012). As predicted, Shh transcripts were markedly reduced in YFP$^+$ pancreatic epithelial cells from ShhPKCY mice (Figure 1B).

Interestingly, this decrease in Shh transcription was accompanied by a 10-fold increase in the expression of Indian hedgehog (Ihh), another Hh ligand, although absolute levels of Ihh remained significantly lower than Shh. Desert hedgehog was undetectable under all conditions (data not shown). We then determined the impact of Shh deletion on signaling within the stromal compartment by measuring the expression of the Hh target genes Ptch1 and Gli1 in sorted PDAC-associated F4/80$^+$ monocytes and whole pancreas, as previously described (El-Zaatari et al., 2013). Although Ptch1 expression was similar, transcript levels for Gli1 were significantly decreased in ShhPKCY samples as compared to PKCY samples, indicating that overall Hh signaling was reduced following Shh deletion (Figure 1B).

Given the important role of Shh in promoting the desmoplastic stroma of PDAC, we expected that Shh loss would impair tumorigenesis. Surprisingly, however, pancreatic tumors arose in both PKCY and ShhPKCY mice, demonstrating that Shh is dispensable for tumorigenesis. Remarkably, ShhPKCY mice developed tumors earlier and had a significantly decreased survival compared to PKCY mice ($p < 0.001$ by log rank [Mantel-Cox] test; Figure 1C). Specifically, ShhPKCY mice had a median survival of 3.61 ± 1.97 months as compared to a median survival of 6.17 ± 2.65 months for PKCY mice (Figure S1B). Heterozygous *Shh$^{fl/+}$;Pdx-Cre; Kras$^{LSL\text{-}G12D/+}$;p53$^{fl/+}$;Rosa26$^{LSL\text{-}YFP}$* (*Shh$^{fl/+}$*PKCY) mice that retained one copy of *Shh* also had reduced median survival compared to PKCY mice (4.14 ± 1.57 months, $p = 0.004$; Figure S1B). ShhPKCY tumors were more aggressive than PKCY tumors, because mean survival from first detection of tumor was significantly shorter in ShhPKCY mice (19.2 ± 5.27 versus 6.5 ± 2.7 days, $p < 0.001$; Figure 1D), and the frequency of gross metastasis was higher in ShhPKCY mice than in PKCY mice (43.4 versus 15.3%, $p = 0.039$ by chi-squared test; Figure 1E), although the tissue distribution of macrometastases was similar (Figure S1C). Moreover, histological analysis revealed a higher frequency of acinar-to-ductal metaplasia (ADM) and pancreatic intraepithelial neoplasia (PanIN) of all grades in 8-week-old ShhPKCY compared to PKCY mice (Figure 1F). These data indicate that Shh is not merely dispensable for pancreatic tumorigenesis, but that it somehow restrains tumor progression and aggressiveness.

Shh Loss Is Associated with Changes in Stromal Composition

Next, we compared the histology of ShhPKCY and PKCY tumors. In contrast to the well-differentiated to moderately differentiated histology of most PKCY tumors, ShhPKCY tumors exhibited predominantly undifferentiated and poorly differentiated histology, with few of the ductal elements observed in most PKCY and human pancreatic tumors (Figures 2A and 2B; Figure S2A). ShhPKCY tumors also exhibited a significant increase in Zeb1 and Slug expression, two markers of epithelial-to-mesenchymal transition, consistent with the predominance of poorly differentiated and undifferentiated histology (Singh et al., 2009; Watanabe et al., 2009) (Figure S2B; $p < 0.05$).

Using the YFP lineage label to distinguish epithelial-derived cancer cells from mesenchyme-derived stromal cells, we found that Shh-deficient tumors had significantly reduced stroma, as indicated by decreased numbers of YFP-negative alpha smooth muscle actin (SMA)-positive myofibroblasts (3.7% ± 0.7% versus 16.7% ± 3.2% of all DAPI+ cells within pancreas tumors; $p = 0.016$; Figures 2C and 2D). Despite their increased aggressiveness (but consistent with stromal loss), ShhPKCY tumors exhibited a trend toward decreased weight (Figure S1B). In addition, ShhPKCY tumors had fewer CD45$^+$ myeloid cells (4.9% ± 0.9% versus 36.7% ± 5.2%; $p = 0.0039$; Figures 2E and 2F) and F4/80$^+$ monocytes (2.8% ± 0.5% versus 15.5% ± 2.7%; $p = 0.010$; Figures 2G and 2H). Indeed, the stromal cell composition of ShhPKCY tumors was similar to that of normal pancreas tissue from *Pdx1-Cre;Rosa26$^{LSL\text{-}YFP/+}$* mice (data not shown). These results demonstrate that robust tumor formation can occur in the absence of a fibroblast- and leukocyte-rich desmoplastic stroma.

Because ShhPKCY tumors progressed more rapidly than their PKCY counterparts, we hypothesized that parallel but opposite changes in tumor vasculature might influence tumor growth. Hence, we examined the endothelial compartment in tumors with and without Shh by CD31 staining. Consistent with this hypothesis, ShhPKCY tumors exhibited a substantial increase in the number of blood vessels within the tumor (32.4 ± 7.2 versus 11.2 ± 3.8 CD31$^+$ vessels per high powered field; $p = 0.0004$; Figures 3A and 3B). In addition, the autofluorescent drug doxorubicin was delivered more effectively to ShhPKCY tumors, suggesting that increased vascular density was accompanied by greater perfusion (Figures 3C and 3D). To assess whether this increase in vasculature was associated with changes in autophagy or proliferation, we stained for the autophagosome marker LC3 and the proliferation marker proliferating cell nuclear antigen (PCNA). This analysis revealed a decrease in YFP$^+$LC3$^+$ cells in ShhPKCY tumors (Figures 3E and 3F) and an increase in the frequency of YFP$^+$PCNA$^+$ proliferating tumor cells (Figures 3G and 3H). These data therefore suggest that undifferentiated ShhPKCY tumors are better perfused than PKCY tumors, a change that was associated with enhanced nutrient delivery, decreased autophagy, and increased proliferation.

Chronic Smoothened Inhibition Phenocopies Shh Deletion

We next sought to learn whether the effect of Shh deletion in pancreatic cancer is mediated by canonical Hh signaling. We utilized IPI-926 (Infinity Pharmaceuticals), a targeted inhibitor of Smo, to inhibit canonical Hh signaling in KPC mice (a PDAC model closely related to the PKCY model). We previously performed a preclinical evaluation of IPI-926 in KPC mice harboring large (6–9 mm) pancreatic tumors and found that the combination of IPI-926 and the nucleoside analog gemcitabine (gem) resulted in extension of overall survival (Olive et al., 2009), a finding at odds with the observed effect of genetic Shh deletion. We reasoned that long-term, chronic exposure to Smo inhibition might unveil indirect responses related to the depletion of stroma from tumors rather than the acute response to improved drug delivery. Therefore, we treated KPC mice with IPI-926 alone or vehicle beginning at 8 weeks of age, a time point at which ADM and PanIN lesions are present but at which mice have not yet developed tumors (Figure S3A; see Supplemental Experimental Procedures for additional details).

Strikingly, IPI-926-treated KPC mice exhibited a reduction in overall survival compared to vehicle-treated mice (121 versus 156 days, $p < 0.0001$ by log rank test; Figure 4A). This result

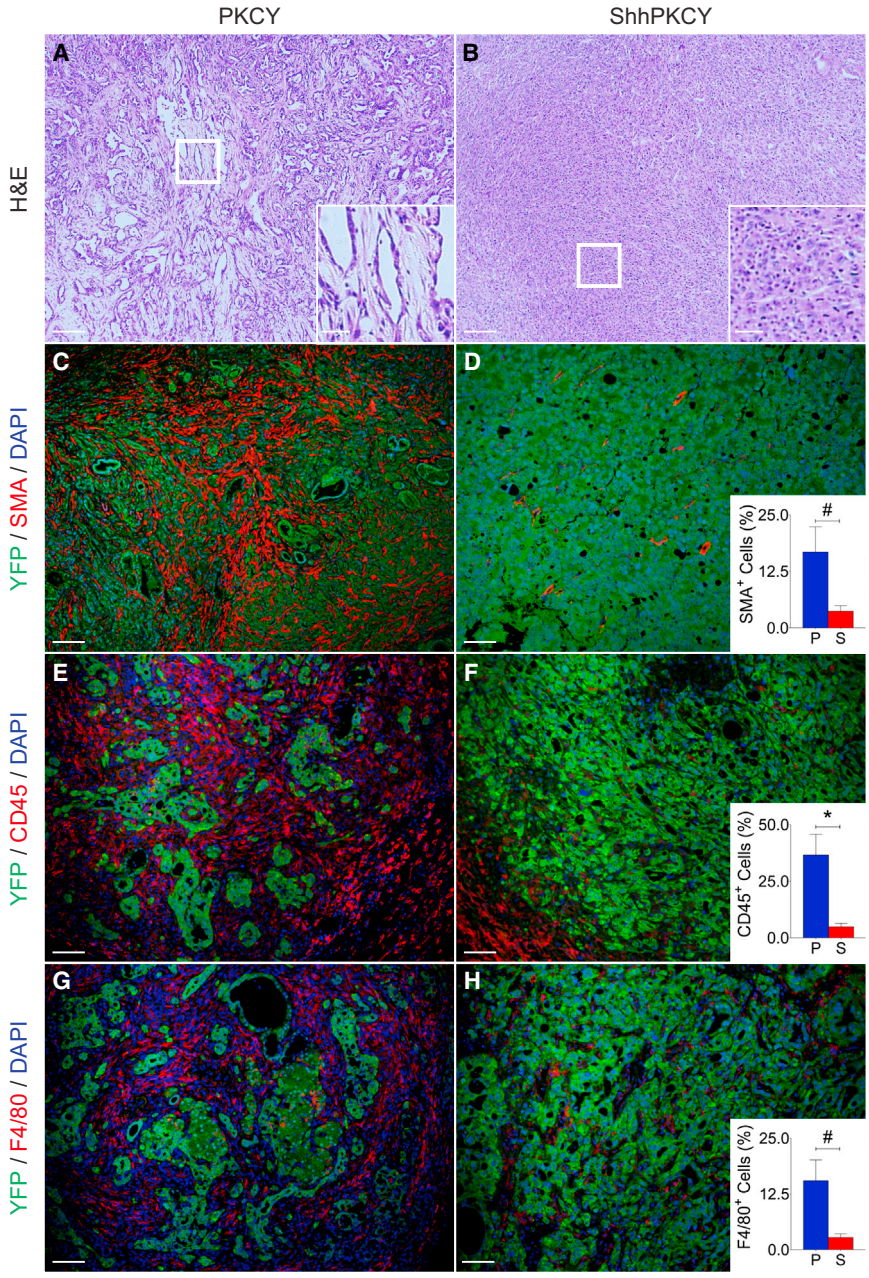

Figure 2. Loss of Shh Leads to a Shift in Pancreatic Tumor Histopathology

(A and B) H&E staining showing representative histology from PKCY (A) and ShhPKCY (B) tumors. Insets show higher magnified view of sections marked by the box.

(C–H) Multicolor immunofluorescence images of PKCY (left column) and ShhPKCY tumors (right column) assessed for myofibroblasts (C and D), total leukocytes (E and F), or macrophages (G and H).

(C and D) Fluorescent images showing staining with the pancreas epithelial lineage label YFP (green) and the myofibroblast marker alpha-SMA (red). Inset, quantitation of SMA+ cells as a percentage of all nucleated (DAPI+) cells within PKCY (blue) and ShhPKCY (red) tumors (n = 3–5; #, p = 0.016; bars represent means ± SD).

(E and F) Fluorescent images showing staining with YFP (green) and the pan-leukocyte marker CD45 (red). Inset, quantitation of $CD45^+$ cells as a percentage of all nucleated ($DAPI^+$) cells (n = 3–5; *, p = 0.0039; bars represent means ± SD).

(G and H) Fluorescent images showing staining with YFP (green) and the macrophage marker F4/80 (red). Inset, quantitation of $F4/80^+$ cells as a percentage of all nucleated (DAPI+) cells (n = 3–5; #, p = 0.010; bars represent means ± SD).

Scale bars, 40 μm for main panels and 20 μm for insets. See also Figure S2.

diverged dramatically from those obtained in our previous intervention study (Olive et al., 2009), despite the fact that the model, drug, dose, route, and schedule were all identical. In an effort to replicate this result and also determine whether coadministration of gemcitabine might change the dynamics of tumor response, we treated a separate cohort of mice with the combination of gemcitabine + IPI-926 or gemcitabine + vehicle. As shown in Figure 4B, the addition of gemcitabine provided a minor extension of survival over IPI-926 monotherapy (p = 0.01, log rank), but the IPI-926-gem combination therapy still resulted in shortened survival compared to vehicle-treated mice from the previous cohort. These results suggest that any benefit afforded by improved drug availability following Smo inhibition is outweighed by other effects on tumor biology in the chronic setting.

Analysis of 3D high resolution ultrasound data (Sastra and Olive, 2013) demonstrated that KPC mice treated with IPI-926 or IPI-926-gemcitabine succumbed more rapidly following initial tumor detection (Figure 4C) and that tumor size was significantly smaller at sacrifice (Figure 4D), similar to the reduced tumor weight observed in ShhPKCY mice (Figure S1B). Indeed, several mice met endpoint criteria before it was possible to detect tumors in their pancreas by ultrasound. However, all but one of these mice was found to have tumors upon careful histopathological analysis. There was no difference in the age at which tumors developed between the two groups, suggesting that IPI-926 treatment accelerates tumor progression after initiation without reducing latency (Figure 4E). Complete tumor volume data for these mice are presented in Figures 4F and 4G.

To better understand why IPI-926-treated mice with very small tumors were dying, we performed detailed necropsies on each mouse and assigned a "proximal cause of death" to each animal. Vehicle- or gem-treated KPC mice typically succumbed to the consequences of locally destructive disease (e.g., local invasion into the gut or abdominal hemorrhage) or high metastatic burden, with only a small subset exhibiting severe weight loss. By contrast, nearly all of the IPI-926-treated mice were euthanized following a period of rapid and severe weight loss

Please cite this article in press as: Rhim et al., Stromal Elements Act to Restrain, Rather Than Support, Pancreatic Ductal Adenocarcinoma, Cancer Cell (2014), http://dx.doi.org/10.1016/j.ccr.2014.04.021

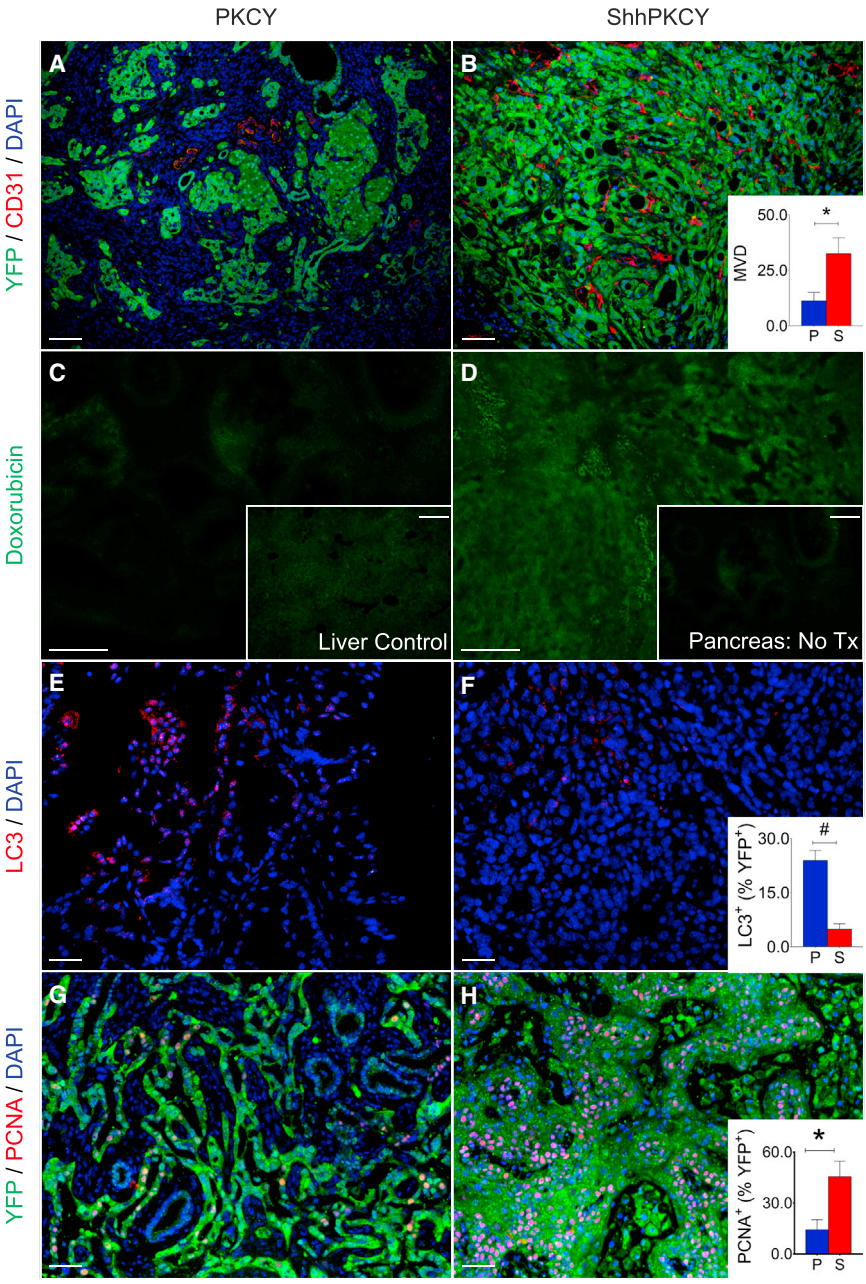

Figure 3. Shh Deletion Results in Greater Vascular Density and Proliferation within Pancreatic Tumors

(A and B) Blood vessel density in PKCY and ShhPKCY tumors was determined by staining for the endothelial marker CD31 (red) and the tumor cell lineage marker YFP (green). Inset, measurement of mean vascular density (MVD) within PKCY (blue) and ShhPKCY (red) tumors (quantified as number of $CD31^+$ vessels per high powered field; n = 3–5; *, p = 0.004; bars represent means ± SD). No Tx, no treatment.

(C and D) Cellular perfusion in PKCY and ShhPKCY tumors was determined by intravascular delivery of the autofluorescent drug doxorubicin. The inset in C shows fluorescence of a liver section from the same PKCY mouse (positive control). The inset in D shows fluorescence of a ShhPKCY tumor injected with PBS (negative control).

(E and F) Autophagy in PKCY and ShhPKCY tumors was determined by staining for the autophagosomal protein LC3 (red). Inset, percentage of $LC3^+$ cells within the YFP^+ tumor cell population in PKCY (blue) and ShhPKCY (red) tumors (n = 3–5; #, p = 0.002; bars represent means ± SD).

(G and H) Proliferation in PKCY and ShhPKCY tumors was determined by staining for the cell cycle marker PCNA (red). Inset, percentage of $PCNA^+$ cells within the YFP^+ tumor cell population in PKCY (blue) and ShhPKCY (red) tumors (n = 3–5; *, p = 0.004; bars represent means ± SD). Scale bars, 40 μm.

(Figures S3B and S3C), a phenomenon also observed in ShhPKCY animals (data not shown).

The tumors arising in IPI-926-treated mice were more poorly differentiated than those arising in controls treated with vehicle or gem alone (Figures 5A–5F), consistent with the observation that ShhPKCY mice developed poorly differentiated tumors. It is worth highlighting a pair of noteworthy exceptions that emphasize the relationship between differentiation state and tumor progression: one IPI-926-treated tumor was extremely well-differentiated and progressed slowly, whereas one vehicle-treated mouse succumbed at an early time point from a small tumor that was 50% poorly differentiated (Figure 4F, highlighted). Examination of pancreatic tissues adjacent to the tumors revealed an exceptionally high content of ADMs and PanINs in IPI-926-treated mice (Figures S4A–S4D). This feature was not shared in IPI-926+gemcitabine-treated mice, possibly because of the impact of genotoxic chemotherapy on the proliferation of preneoplastic lesions. Immunohistochemical analyses revealed that IPI-926-treated tumors were more highly proliferative (Figure 5G; Figures S4E–S4H) and had increased vascular content (Figure 5H; Figures S4I–S4L). Together, these data demonstrate that pharmacologic inhibition of canonical Hedgehog signaling accelerates tumor growth, phenocopying the effect of genetic deletion of Shh in pancreatic tumors.

Hedgehog Signaling Acts in a Paracrine Fashion in PDAC

During embryonic endoderm development, Hedgehog ligand is secreted by gut epithelial cells and acts on adjacent mesenchymal cells to pattern the submucosal layers of the gut (Roberts et al., 1998; Sukegawa et al., 2000). Given strong evidence from previous literature that Hedgehog signaling acts in a paracrine fashion during pancreatic carcinogenesis (Bailey et al., 2008; Tian et al., 2009), we sought to determine whether a similar signaling relay was operating in the autochthonous models. To this end, we introduced a *Gli1*^{GFP} reporter (Brownell et al., 2011) into the KPC background and assessed the distribution

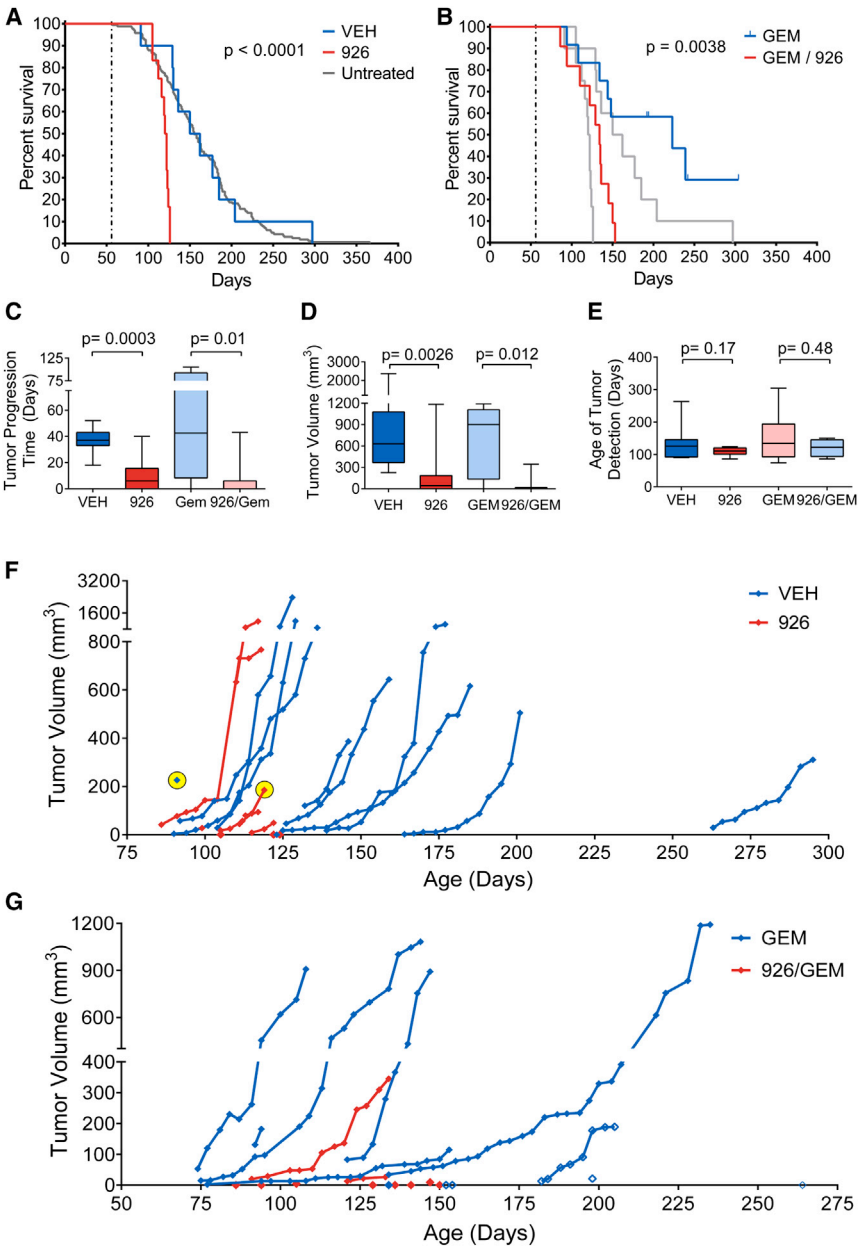

Figure 4. Smoothened Inhibition Accelerates Pancreatic Tumor Development

(A–G) Two separate cohorts of KPC mice were treated with vehicle (VEH) versus IPI-926 (926), or gemcitabine (GEM) versus IPI-926 + gemcitabine (926/GEM), beginning at 8 weeks of age, as described in Supplemental Experimental Procedures. High resolution 3D ultrasound was used to monitor tumor development and to quantify tumor volumes. Treatment continued until mice met endpoint criteria.

(A) Kaplan-Meier curve showing IPI-926 treated KPC mice (red, n = 12), vehicle-treated KPC mice (blue, n = 12) ($p < 0.0001$, log rank test, vehicle versus IPI-926), and an historical collection of untreated KPC mice (gray, n = 165) ($p < 0.0001$, log rank test, historical cohort versus IPI-926).

(B) Kaplan-Meier curve showing IPI-926 + gemcitabine-treated KPC mice (red, n = 11) and vehicle + gemcitabine-treated KPC mice (blue, n = 12) ($p < 0.004$, log rank test, gemcitabine + vehicle versus gemcitabine + IPI-926). The data from panel A are overlaid in gray ($p = 0.01$, log rank test, IPI-926 versus IPI-926 + gemcitabine).

(C) Graph of time from first detection of tumor (by 3D ultrasound) to death in animals among the four treatment groups, comparing animals that received IPI-926 to those that did not ($p = 0.0003$ in monotherapy group, $p = 0.006$ in combination group). Animals with microscopic tumors on necropsy but no measurable tumor on ultrasound were included as 0 days. The data are presented as standard box and whisker plots.

(D) Final tumor volumes (measured by 3D ultrasound) among the four treatment groups, comparing animals that received IPI-926 to those that did not ($p = 0.0026$ in monotherapy group, $p = 0.012$ in the combination group). Several IPI-926-treated mice met endpoint criteria prior to the detection of tumors by ultrasound and are included as 0 mm^3. The data are presented as standard box and whisker plots.

(E) Age of tumor detection (by 3D ultrasound) among the four treatment groups ($p = 0.17$ for monotherapy, $p = 0.48$ for combination). The data are presented as standard box and whisker plots.

(F) Graph showing tumor volumes of mice treated with IPI-926 (red) or vehicle (blue) plotted versus the mouse's age in days. Two exceptional tumors noted in the text are highlighted in yellow.

(G) Graph showing tumor volumes of mice treated with gemcitabine + IPI-926 (red) or gemcitabine + vehicle (blue) are plotted versus the mouse's age in days. Lethal tumors that were undetectable by ultrasound were assigned a volume of 0 on the day of death. Animals still alive at the time of submission are denoted with open diamonds.

See also Figure S3.

of GFP^+ cells in the resulting KPC-$Gli1^{GFP}$ mice by immunofluorescence. GFP staining was readily observed in the E-cadherin-negative (stromal) portions of KPC-$Gli1^{GFP}$ mice but was absent from E-cadherin-positive (epithelial) cells (Figures 6A and 6B). Consistent with this observation, spheroid formation of a KPC pancreatic tumor cell line was unaffected by treatment with recombinant Shh protein or IPI-926 (Figure S5A). In contrast, nearly all alpha-SMA^+ myofibroblasts were found to be $Gli1^{GFP}$ positive, indicating active Hh pathway signaling in this mesenchymally derived cell type (Figures 6A and 6C). This is consistent with previous reports demonstrating a proliferative effect from Hh pathway signaling in fibroblasts (Walter et al., 2010). However, further examination of these tissue sections revealed that many $Gli1^{GFP}$-positive cells (43%) were alpha-SMA negative (Figures 6A and 6C), indicating that multiple stromal cell types can respond to Hh signaling. Importantly, treatment of KPC-$Gli1^{GFP}$ mice with IPI-926 for 10 days completely abrogated GFP staining, indicating that GFP staining was accurately reporting canonical Hedgehog signaling (Figures 6D and 6E). Taken together, these experiments confirm that canonical Hh signaling

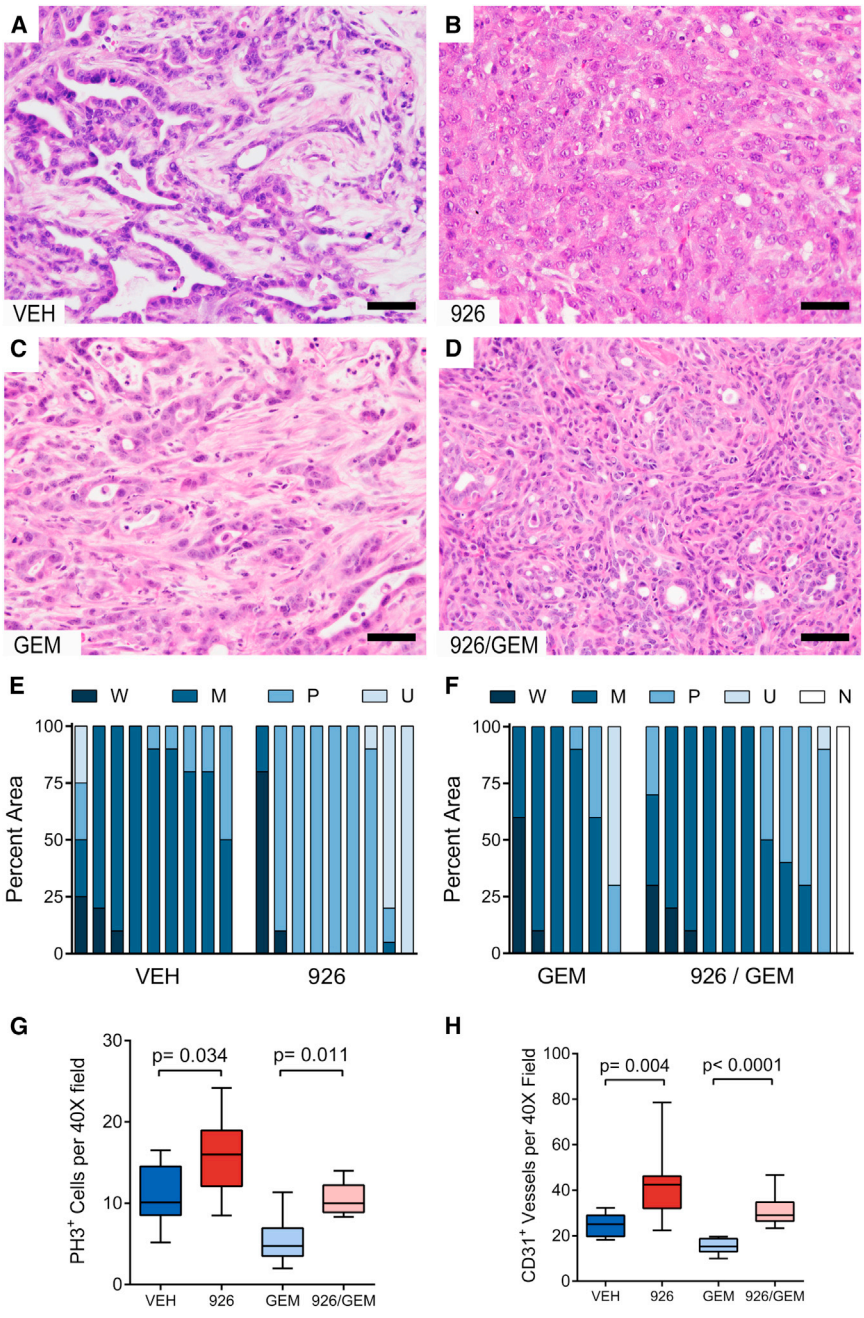

Figure 5. Long-Term Smoothened Inhibition Yields Poorly Differentiated Pancreatic Tumors with Increased Proliferation and Vascularity

(A–D) Representative histology (hematoxylin and eosin stain) of KPC tumors arising after long-term treatment with vehicle (A, VEH), IPI-926 (B), gemcitabine + vehicle (C), or gemcitabine + IPI-926 (D).

(E and F) Quantification of the differentiation state for each cohort. The fraction of each tumor that was observed to be well-differentiated (W), moderately differentiated (M), poorly differentiated (P), or undifferentiated (U) was scored in a blinded manner, and compared between the treatments. No tumor could be located in one IPI-926 + gemcitabine-treated mouse (N).

(G) Quantification of phospho-histone $H3^+$ cells per 40[times] field in each treatment group ($p = 0.034$ for monotherapy, $p = 0.011$ for combination). The data are presented as standard box and whisker plots.

(H) Quantification of $CD31^+$ vessel structures by IHC in each treatment cohort ($p = 0.004$ for monotherapy, $p < 0.0001$ for combination). The data are presented as standard box and whisker plots. Two-tailed Mann-Whitney U tests were used for all unpaired tests. Scale bars, 50 μm. See also Figure S4.

operates in a paracrine fashion in PDAC, as it does during embryonic development.

Shh-Deficient Tumors Are Sensitive to VEGF Inhibition

We next investigated the surprising increase in vasculature in ShhPKCY mice and in IPI-926-treated KPC mice. We first sought to determine whether increased angiogenesis was a direct result of reduced Hh pathway signaling in endothelial cells. We performed coimmunofluorescence on untreated KPC-$Gli1^{GFP}$ mice for GFP and the endothelial marker endomucin but found that Hh pathway signaling is absent in nearly all tumor endothelial cells (Figures 6A and 6F). Consistent with this observation, capillary sprouting of cultured human umbilical venous endothelial cells was unaffected by exposure to recombinant Shh or IPI-926 (Figure S5B). These results suggest that the proangiogenic effect of Hh pathway inhibition is mediated indirectly by signals from mesenchyme-derived stromal cells.

VEGF is a well-known soluble angiogenic factor. As a group, mouse and human PDAC are unaffected by treatment with VEGF receptor inhibitors, consistent with their poor vascularization (Singh et al., 2010). However, undifferentiated tumors comprise approximately 5%–10% of all advanced PDAC (Iacobuzio-Donahue et al., 2009). We hypothesized that the higher vessel density and paucity of stroma of undifferentiated tumors might render them sensitive to angiogenesis inhibitors. To test this hypothesis, we treated tumor-bearing ShhPKCY and control PKCY mice with DC101, a blocking antibody against VEGFR2. Similar to previous studies (Singh et al., 2010), VEGFR inhibition had little effect on tumor size or survival in PKCY mice (Figure 7A; Figure S6A). However, treatment of ShhPKCY mice with DC101 led to significantly improved overall survival compared to treatment with Ig control (median survival 22.4 versus 12.5 days from enrollment; $p = 0.028$; Figure 7B). DC101 treatment was associated with the appearance of large areas of necrosis on hematoxylin and eosin (H&E) (Figures 7C and 7D), and immunofluorescence staining demonstrated a reduced

A

Gli1-GFP$^+$ / E-Cadherin$^+$	11
Total E-Cadherin$^+$ Cells Counted	968
% Double Positive	1.14%

Gli1-GFP$^+$ / Blood Vessel	9
Total Blood Vessels Counted	400
% Double Positive	2.25%

Gli1-GFP/SMA	Total: 496	
Gli1-GFP$^+$ SMA$^+$	Gli1-GFP$^+$ SMA$^-$	Gli1-GFP$^-$ SMA$^+$
276	217	3
55.65%	43.75%	0.60%

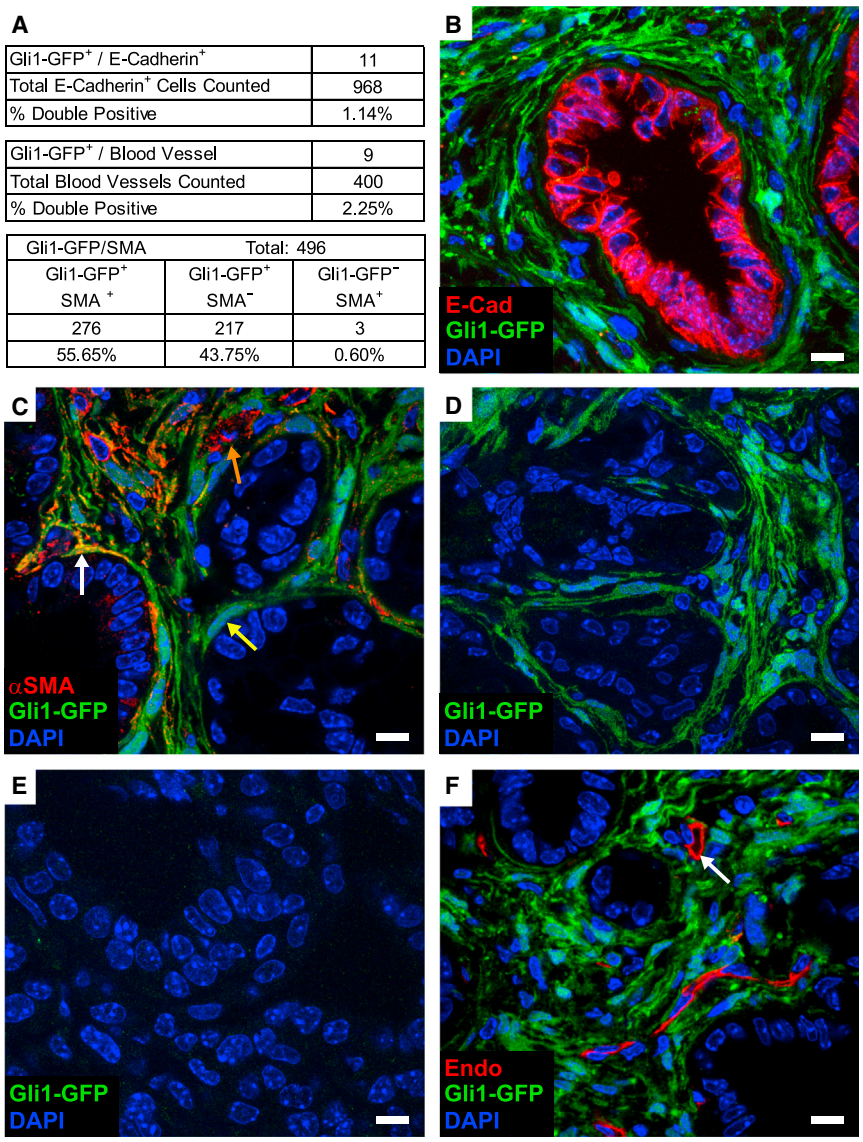

Figure 6. Hh Pathway Activity Is Restricted to Mesenchymally Derived Stromal Cells

(A) Quantification of coimmunofluorescence (Co-IF) for the Gli1^{GFP} Hh reporter and markers of various tumor and stromal populations.

(B) Co-IF for Gli1^{GFP} (green) and E-Cadherin (red, E-Cad) in KPC-Gli1^{GFP} tumors.

(C) Co-IF for Gli1^{GFP} (green) and alpha-SMA (red, αSMA) in in KPC-Gli1^{GFP} tumors. White arrow denotes an alpha-SMA$^+$, Gli1$^+$ cell. Yellow arrow denotes an alpha-SMA$^-$, Gli1$^+$ cell. Orange arrow denotes an aSMA$^+$, Gli1$^-$ cell.

(D and E) Co-IF for Gli1^{GFP} reporter on an untreated KPC-Gli1^{GFP} tumor (D) or after 10 days of IPI-926 treatment (E).

(F) Co-IF for Gli1^{GFP} (green) and the endothelial marker endomucin (red, Endo) in KPC-Gli1^{GFP} tumors. Arrow denotes a Gli1$^-$ endothelial cell.

Scale bars, 10 μm. See also Figure S5.

number of CD31$^+$ blood vessels (Figure 7E; Figures S6B and S6C), an increase in the percentage of tumor cells with LC3$^+$ autophagosomes (Figure 7F; Figures S6D and S6E), and reduced proliferation (Figure 7G; Figures S6F and S6G) in DC101-treated ShhPKCY mice. Interestingly, there was no difference in tumor VEGF expression between ShhPCKY versus PKCY mice or between IPI-926- versus vehicle-treated KPC tumors (data not shown). Thus, the depletion of Hh-dependent stroma from pancreatic tumors leads to a greater utilization and dependence on existing VEGF-mediated angiogenic pathways rather than a de novo induction of VEGF ligand.

Finally, we examined human pancreatic tumors to determine whether similar relationships between histology, Hedgehog signaling, and vascularity were present. In a set of 225 prospectively collected and analyzed human PDAC, undifferentiated tumors had significantly less Gli1 expression compared to all other tumors with well, moderately, and poorly differentiated histology (1.42 versus 2.99; p = 0.0102 by Student's t test, two-tailed; Figure S6H). However, no statistically significant difference was detected in Shh expression. Thus, undifferentiated human PDAC may be associated with attenuated canonical Hedgehog signaling, as predicted by our studies of genetically engineered mice. In a separate, independently collected and analyzed set of human PDAC, we examined 13 total human pancreatic tumors stratified into differentiated (n = 5) and undifferentiated (n = 8) histology to determine whether differentiation status correlated with vessel density in patients. Similar to mice, undifferentiated human pancreatic tumors exhibited significantly greater vascular density and less stroma compared to differentiated tumors, even when both components were present within the same primary carcinoma (Figures 7H–7J). Surprisingly, undifferentiated PDAC had a similar vascular density as normal human pancreas tissue (Figure 7J). These data indicate that like murine ShhPKCY tumors, undifferentiated pancreatic tumors in patients also have a more prominent vasculature.

DISCUSSION

Nearly 50 years have passed since Stoker's pioneering studies of epithelial/stromal interactions in cancer demonstrated that normal fibroblasts restrain the growth of transformed baby hamster kidney cells (Stoker et al., 1966). This "neighbor suppression" effect may be part of an evolved microenvironment surveillance against the development of preneoplasia (Klein, 2014). Nevertheless, in the context of established tumors, the prevailing paradigm of the tumor microenvironment field has been that tumor stroma supports, rather than inhibits, neoplastic growth and progression (Hanahan and Weinberg, 2011). This concept has been bolstered by work on pancreatic

tumors, which are associated with a particularly dense "desmoplastic" stroma. Such studies, which have mostly relied on cell transplantation or in vitro assays, have affirmed that the stroma plays a supportive role in of pancreatic cancer progression (Bailey et al., 2008; Feldmann et al., 2008a, 2008b; Hwang et al., 2008; Ikenaga et al., 2010; Lonardo et al., 2012; Xu et al., 2010). In this study, we have examined the effects of perturbing the tumor microenvironment by genetically deleting sonic hedgehog or pharmacologically inhibiting its essential signaling mediator Smoothened. These interventions greatly reduced stromal desmoplasia, but such tumors unexpectedly exhibited accelerated tumor growth, increased systemic morbidity, and increased metastasis, ultimately leading to earlier mortality. Thus, our findings demonstrate that at least some stromal constituents can act to restrain, rather than promote, tumor progression.

We previously reported that acute administration of IPI-926 to KPC mice bearing large tumors leads to stromal collapse and increased vascularity, consistent with the results shown here (Olive et al., 2009). In that study, treatment with Smo inhibitor alone had minimal effects on tumor size or survival, whereas combined treatment with the Smo inhibitor and gemcitabine led to transient stabilizations and regressions, producing a modest survival benefit (Olive et al., 2009). These results were interpreted as an indication that stromal inhibition could lead to improved drug delivery without a direct effect on tumor growth. However, because most animals in our previous study experienced less than 3 weeks of IPI-926 treatment, there was little opportunity to detect accelerated tumor progression in this acute setting. Indeed, despite the success of IPI-926 in treating basal cell carcinoma (Jimeno et al., 2013), the poor clinical performance of Smo inhibitors in pancreatic cancer trials has led to uncertainty regarding the approach of stromal targeting. Our current data suggest that the short-term, beneficial effects of increased drug delivery are eventually overcome by the negative effects of long-term Smo inhibition.

What is responsible for the increase in tumor cell proliferation and overall mortality in ShhPKCY (and IPI-926-treated) tumors? At present, the precise mechanism for increased tumor cell proliferation remains unknown and is likely to be complex. Nevertheless, the nearly 3-fold increase in blood vessel density in ShhPKCY tumors compared to PKCY tumors—an association that has been previously observed in IPI-926-treated KPC mice (Olive et al., 2009)—is likely to be a major contributor to this effect. This inference is supported by the observation that the more vascular ShhPKCY tumors had a nearly 5-fold decrease in autophagy, a process of cellular autodigestion used by nutrient-deprived cells (Kondo et al., 2005). Moreover, ShhPKCY tumors exhibited a responsiveness to antiangiogenic therapy that was absent in PKCY tumors, suggesting that the more highly vascular Shh-deficient tumors were dependent on this enhanced blood supply. Thus, our study suggests that the interaction between the tumor and its microenvironment is complex, with certain components of the microenvironment (i.e., vasculature) having a tumor-promoting role and other components (i.e., myofibroblasts) having an inert or tumor-suppressive role.

A paradoxical result of our study was the observation that the tumors lacking Hedgehog signaling—following either genetic ablation or treatment with IPI-926—were smaller despite their more aggressive and lethal phenotype, a finding that may reflect the fact that the stroma normally comprises a large percentage of PDAC tumor volume (Chu et al., 2007). Although we do not fully understand the accelerated mortality of Shh-deficient tumors, one possibility is suggested by the finding that tumor-bearing animals treated with IPI-926 exhibited significantly more weight loss and wasting prior to death than vehicle- or gem-treated tumors. It is conceivable that stromal inhibition (and associated changes in tumor metabolism) may lead to increased cachexia, a wasting syndrome common in human PDAC patients. Importantly, we do not believe that IPI-926 contributes to increased mortality or wasting independent of PDAC, because extensive clinical follow-up (Jimeno et al., 2013) and our own observations treating tumor-free animals (data not shown) failed to demonstrate any such toxicity.

There are several models that could account for the finding that ShhPKCY tumors have a reduction in myofibroblasts and leukocytes and an increase in blood vessels. Our data demonstrate that Hh signaling is nearly absent in the endothelial population, arguing against a direct role in angiogenesis. Rather, our findings are consistent with a model in which mesenchymal stromal cells exert an antiangiogenic effect on endothelial cells, possibly acting either directly or indirectly to elevate interstitial fluid pressure, which then represses blood vessel growth (Jacobetz et al., 2013; Provenzano et al., 2012). Importantly, these possibilities are not mutually exclusive, and future studies will be needed to understand the nature of cellular crosstalk between different components of the microenvironment and the role that Shh plays in each.

It is worth noting that global deletion of Gli1, a known mediator of Hedgehog signaling, completely blocks the development of $Kras^{G12D}$-driven pancreatic tumors (Mills et al., 2013). However, because Gli1 can be activated by signals other than Smoothened, it is unclear whether this reported requirement for Gli1 is due to so-called "canonical" (Smo-mediated) Hedgehog signaling or is mediated by other Gli1-dependent signaling pathways. Moreover, because the $Gli1^{GFP}$ reporter showed little if any activity within the tumor epithelium, it is unlikely that the effects we observed are due to a Hh-Smo-Gli1 signaling relay within the tumor cells themselves. Importantly, we employed autochthonous models that harbor mutant *Kras* and *p53*—mutations that are present in 95% and 75%–90% of human PDAC patients, respectively—and it remains to be determined whether the observed effects of Hedgehog deficiency on tumor biology occur only in the context of these genetic lesions or are more generalizable.

It is remarkable that the genetic or pharmacologic manipulation of Hedgehog signaling was associated with a dramatic change in tumor histology, illustrating the high degree of plasticity of differentiation status that exists within tumors in vivo. These data are corroborated by our analysis of human pancreatic tumors. Because poorly differentiated histopathology is strongly associated with poor outcome in PDAC (Han et al., 2006; Yonemasu et al., 2001), this finding has potential clinical implications. Specifically, the observation that inhibition of the Hedgehog pathway leads to the development of less differentiated and more aggressive tumors may explain the lack of benefit observed in clinical trials.

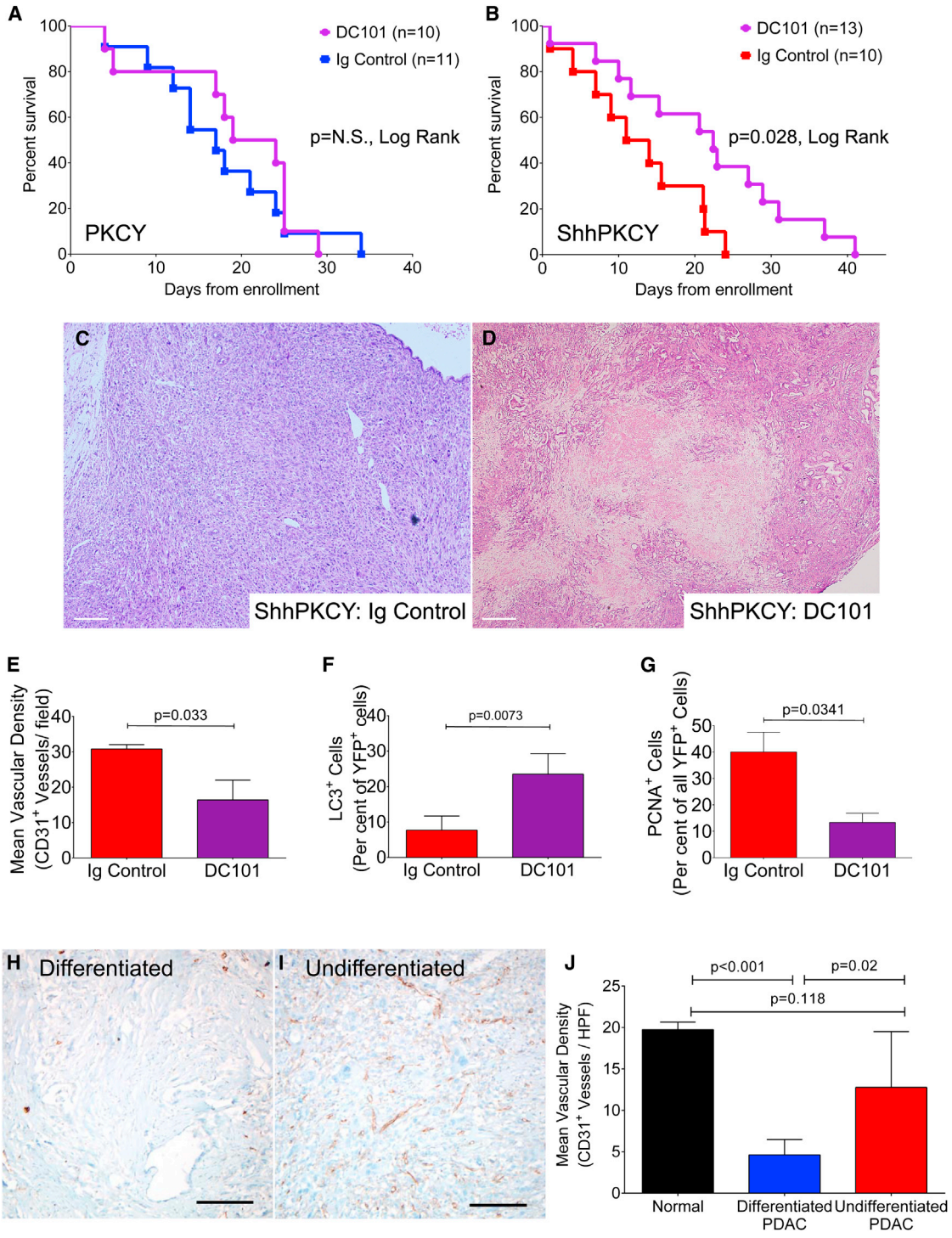

Figure 7. VEGFR2 Antagonism Leads to Selective Inhibition of Tumor Growth in ShhPKCY Mice

(A) Kaplan-Meier survival curve for tumor-bearing PKCY mice treated with bi-weekly DC101 (purple, n = 10) or Ig control (blue, n = 11).

(B) Kaplan-Meier survival curve for tumor-bearing ShhPKCY mice treated with bi-weekly DC101 (purple, n = 13) or Ig control (red, n = 10).

(C and D) H&E analysis of ShhPKCY tumors showing a large area of necrosis upon DC101 treatment (D). Scale bars, 250 μm.

(E) Quantification of $CD31^+$ vessel density in ShhPKCY mice treated with DC101 compared to Ig control, depicted as mean (±SD) number of $CD31^+$ vessels per high powered field (n = 3–5).

(F) Quantification of YFP^+ cells containing $LC3^+$ autophagosomes in ShhPKCY mice treated with DC101 compared to Ig control, depicted as percentage (±SD) of YFP^+ tumor cells exhibiting LC3 staining (n = 3–5).

(legend continued on next page)

Finally, our discovery that undifferentiated tumors were sensitive to VEGFR inhibition points to a possible biomarker of sensitivity to angiogenesis inhibitors in pancreatic cancer. The marked response of ShhPKCY tumors to an antiangiogenesis agent suggests that such undifferentiated tumors are dependent on a plentiful vascular network. Although clinical trials of antiangiogenesis agents failed to show benefit in PDAC, a portion of patients treated with bevacizumab did exhibit a durable response (Kindler et al., 2010). Approximately 5%–10% of advanced human pancreatic tumors exhibit an undifferentiated histology (Iacobuzio-Donahue et al., 2009), and the data we present here suggest that such tumors have a higher blood vessel density. Given our finding that poorly differentiated but well-vascularized pancreatic tumors respond to VEGF receptor blockade, it may be worth reconsidering antiangiogenesis treatment strategies for the subset of patients who harbor predominantly undifferentiated PDAC.

EXPERIMENTAL PROCEDURES

Mouse Models

All studies were conducted in compliance with the institutional guidelines of their respective locations. Two genetically engineered mouse models were used in these studies: *p53*$^{fl/+}$; *Kras*$^{LSL\text{-}G12D/+}$;*Pdx1-Cre;Rosa26*^{YFP} (PKCY) (Rhim et al., 2012) and *Kras*$^{LSL\text{-}G12D/+}$;*p53*$^{LSL\text{-}R172H}$;*Pdx1-Cre* (KPC) (Hingorani et al., 2005). ShhPKCY and PKCY mice were used to determine the effect of Shh deletion in tumorigenesis and cancer progression. KPC mice were used in a chronic treatment trial of IPI-926. The *Gli1*$^{eGFP/+}$ allele was crossed into the KPC mouse for immunofluorescence studies (Brownell et al., 2011).

Analysis of Tumor Progression and Survival in PKCY and ShhPKCY Mice

All experiments involving mice were performed in accordance with relevant institutional and national guidelines and were approved by the institutional animal care and use committees at the University of Pennsylvania, Columbia University, and University of Michigan prior to experimentation. Starting at 2 months of age, mice were palpated twice weekly for evidence of tumor. If a potential mass was appreciated, transabdominal ultrasound was performed using a SonoSite M-Turbo ultrasound. If the presence of a tumor was confirmed, mice were examined weekly using ultrasound and general physical exam. If the mouse appeared moribund (decreased spontaneous physical activity, decreased toe pinch reflex, tachycardia, tachypnea, failure to groom, and ruffled coat), indicating low probability of surviving for greater than 24 hr, it was sacrificed for analysis. The tumors were immediately removed and weighed; the dimensions were measured; and the animals were analyzed for evidence of macrometastatic disease.

In Vivo DC101 T1rial

Upon detection of tumor by ultrasound, ShhPKCY and PKCY mice were randomized to two treatment arms: DC101 or IgG1 control (800 μg per mouse; Bio X Cell, West Hanover, NH) administered intraperitoneally every Monday and Thursday. Technicians were blinded to treatment group.

Analysis of Human Pancreatic Tumors

Studies involving all human pancreas tumors were approved by the institutional review boards of Johns Hopkins University and Mayo School of Medicine, and informed consent was obtained from all patients prior to tissue procurement and subsequent analysis. Paraffin-embedded sections (4 μm thickness) of eight human ductal adenocarcinomas with undifferentiated features from the Johns Hopkins Gastrointestinal Rapid Medical Donation Program (Iacobuzio-Donahue et al., 2009) were used and compared to five conventional PDACs and three samples of normal pancreas. Immunolabeling for CD31 was performed using standard histologic methods with prediluted anti-human CD31 monoclonal antibody (Ventana, clone JC70) and detected using the Dako universal liquid DAB+ substrate chromagen system per the manufacturer's instructions (catalog K3468). Slides were counterstained with hematoxylin for 30 s. Microvascular density was calculated as the number of CD31^{+} vessels per field using a 40[times] objective and a minimum of four fields per sample.

Statistics

All statistics, including Kaplan-Meier statistics (log rank) and results from chi-squared tests, Mann-Whitney U tests, and Student's t tests, were calculated using GraphPad Prism v.5.04 or v.6. The p values from Student's t tests are listed unless otherwise specified. In all graphs, means (bars) and standard deviations (lines) are denoted.

SUPPLEMENTAL INFORMATION

Supplemental Information includes Supplemental Experimental Procedures and six figures and can be found with this article online at http://dx.doi.org/10.1016/j.ccr.2014.04.021.

AUTHOR CONTRIBUTIONS

A.D.R. planned and led all studies using PKCY mice. P.E.O. planned and led the survival study of KPC mice treated with IPI-926. D.H.T. planned and led studies using KPC-Gli1-GFP mice.

ACKNOWLEDGMENTS

We thank E. Collisson, R. Hruban, A. Rustgi, R. Vonderheide, and T. Wang for helpful discussions, as well as B. Orelli, M. Badgley, and J. Eberle for assistance in preparing the manuscript. We also thank Infinity Pharmaceuticals for providing IPI-926 and A. Joyner for providing Gli1-GFP mice. This study was funded by the NIH (DK088945, CA177857, DK034933, and CA046952 [to A.D.R.]; T32CA009503 [to D.H.T.]; CA136526 [to M.E.F.Z.]; CA157980 [to K.P.O.]; and CA169123, DK083355, and DK083111 [to B.Z.S.]) and AGA/FDHN (Fellow to Faculty Transition Award [to A.D.R.] and Bernard L. Schwartz Designated Research Award in Pancreatic Cancer [to K.P.O.]). This work was supported in part by the NIH/NIDDK Center for Molecular Studies in Digestive and Liver Diseases (P30DK050306) and its core facilities (Molecular Pathology and Imaging Core, Molecular Biology/Gene Expression Core, Transgenic and Chimeric Mouse Core, and Cell Culture Core) at the University of Pennsylvania and by the Molecular Pathology Shared Resource, the Confocal and Specialized Imaging Shared Resource, and the Small Animal Imaging Shared Resource within the Columbia University Herbert Irving Comprehensive Cancer Center (P30CA013696). The confocal microscope was purchased with grant S10RR025686.

Received: May 16, 2013
Revised: March 18, 2014
Accepted: April 25, 2014
Published: May 22, 2014

(G) Quantification of YFP^{+} cells staining with the proliferation in ShhPKCY mice treated with DC101 compared to Ig control, depicted as percentage (±SD) of YFP+ tumor cells that were PCNA positive (n = 3 YFP 5).

(H and I) IHC for CD31 in differentiated (H) and undifferentiated (I) portions of human pancreas tumor A21. Scale bars, 200 μm.

(J) Mean vascular density of normal pancreas (n = 3), differentiated human PDAC (n = 5), and undifferentiated human PDAC (n = 8). Bars represent p values by two-sided Student's t test.

See also Figure S6.

REFERENCES

Bailey, J.M., Swanson, B.J., Hamada, T., Eggers, J.P., Singh, P.K., Caffery, T., Ouellette, M.M., and Hollingsworth, M.A. (2008). Sonic hedgehog promotes desmoplasia in pancreatic cancer. Clin. Cancer Res. *14*, 5995–6004.

Brownell, I., Guevara, E., Bai, C.B., Loomis, C.A., and Joyner, A.L. (2011). Nerve-derived sonic hedgehog defines a niche for hair follicle stem cells capable of becoming epidermal stem cells. Cell Stem Cell *8*, 552–565.

Chu, G.C., Kimmelman, A.C., Hezel, A.F., and DePinho, R.A. (2007). Stromal biology of pancreatic cancer. J. Cell. Biochem. *101*, 887–907.

El-Zaatari, M., Kao, J.Y., Tessier, A., Bai, L., Hayes, M.M., Fontaine, C., Eaton, K.A., and Merchant, J.L. (2013). Gli1 deletion prevents Helicobacter-induced gastric metaplasia and expansion of myeloid cell subsets. PLoS ONE *8*, e58935.

Engels, B., Rowley, D.A., and Schreiber, H. (2012). Targeting stroma to treat cancers. Semin. Cancer Biol. *22*, 41–49.

Feldmann, G., Fendrich, V., McGovern, K., Bedja, D., Bisht, S., Alvarez, H., Koorstra, J.B., Habbe, N., Karikari, C., Mullendore, M., et al. (2008a). An orally bioavailable small-molecule inhibitor of Hedgehog signaling inhibits tumor initiation and metastasis in pancreatic cancer. Mol. Cancer Ther. *7*, 2725–2735.

Feldmann, G., Habbe, N., Dhara, S., Bisht, S., Alvarez, H., Fendrich, V., Beaty, R., Mullendore, M., Karikari, C., Bardeesy, N., et al. (2008b). Hedgehog inhibition prolongs survival in a genetically engineered mouse model of pancreatic cancer. Gut *57*, 1420–1430.

Han, S.S., Jang, J.Y., Kim, S.W., Kim, W.H., Lee, K.U., and Park, Y.H. (2006). Analysis of long-term survivors after surgical resection for pancreatic cancer. Pancreas *32*, 271–275.

Hanahan, D., and Weinberg, R.A. (2011). Hallmarks of cancer: The next generation. Cell *144*, 646–674.

Hingorani, S.R., Wang, L., Multani, A.S., Combs, C., Deramaudt, T.B., Hruban, R.H., Rustgi, A.K., Chang, S., and Tuveson, D.A. (2005). Trp53R172H and KrasG12D cooperate to promote chromosomal instability and widely metastatic pancreatic ductal adenocarcinoma in mice. Cancer Cell *7*, 469–483.

Hwang, R.F., Moore, T., Arumugam, T., Ramachandran, V., Amos, K.D., Rivera, A., Ji, B., Evans, D.B., and Logsdon, C.D. (2008). Cancer-associated stromal fibroblasts promote pancreatic tumor progression. Cancer Res. *68*, 918–926.

Iacobuzio-Donahue, C.A., Fu, B., Yachida, S., Luo, M., Abe, H., Henderson, C.M., Vilardell, F., Wang, Z., Keller, J.W., Banerjee, P., et al. (2009). DPC4 gene status of the primary carcinoma correlates with patterns of failure in patients with pancreatic cancer. J. Clin. Oncol. *27*, 1806–1813.

Ikenaga, N., Ohuchida, K., Mizumoto, K., Cui, L., Kayashima, T., Morimatsu, K., Moriyama, T., Nakata, K., Fujita, H., and Tanaka, M. (2010). CD10+ pancreatic stellate cells enhance the progression of pancreatic cancer. Gastroenterology *139*, 1041–1051.

Jacobetz, M.A., Chan, D.S., Neesse, A., Bapiro, T.E., Cook, N., Frese, K.K., Feig, C., Nakagawa, T., Caldwell, M.E., Zecchini, H.I., et al. (2013). Hyaluronan impairs vascular function and drug delivery in a mouse model of pancreatic cancer. Gut *62*, 112–120.

Jimeno, A., Weiss, G.J., Miller, W.H., Jr., Gettinger, S., Eigl, B.J., Chang, A.L., Dunbar, J., Devens, S., Faia, K., Skliris, G., et al. (2013). Phase I study of the hedgehog pathway inhibitor IPI-926 in adult patients with solid tumors. Clin. Cancer Res. *19*, 2766–2774.

Kindler, H.L., Niedzwiecki, D., Hollis, D., Sutherland, S., Schrag, D., Hurwitz, H., Innocenti, F., Mulcahy, M.F., O'Reilly, E., Wozniak, T.F., et al. (2010). Gemcitabine plus bevacizumab compared with gemcitabine plus placebo in patients with advanced pancreatic cancer: Phase III trial of the Cancer and Leukemia Group B (CALGB 80303). J. Clin. Oncol. *28*, 3617–3622.

Klein, G. (2014). Evolutionary aspects of cancer resistance. Semin. Cancer Biol. *25C*, 10–14.

Kondo, Y., Kanzawa, T., Sawaya, R., and Kondo, S. (2005). The role of autophagy in cancer development and response to therapy. Nat. Rev. Cancer *5*, 726–734.

Lonardo, E., Frias-Aldeguer, J., Hermann, P.C., and Heeschen, C. (2012). Pancreatic stellate cells form a niche for cancer stem cells and promote their self-renewal and invasiveness. Cell Cycle *11*, 1282–1290.

Mao, J., Ligon, K.L., Rakhlin, E.Y., Thayer, S.P., Bronson, R.T., Rowitch, D., and McMahon, A.P. (2006). A novel somatic mouse model to survey tumorigenic potential applied to the Hedgehog pathway. Cancer Res. *66*, 10171–10178.

Mills, L.D., Zhang, Y., Marler, R.J., Herreros-Villanueva, M., Zhang, L., Almada, L.L., Couch, F., Wetmore, C., Pasca di Magliano, M., and Fernandez-Zapico, M.E. (2013). Loss of the transcription factor GLI1 identifies a signaling network in the tumor microenvironment mediating KRAS oncogene-induced transformation. J. Biol. Chem. *288*, 11786–11794.

Morton, J.P., Mongeau, M.E., Klimstra, D.S., Morris, J.P., Lee, Y.C., Kawaguchi, Y., Wright, C.V., Hebrok, M., and Lewis, B.C. (2007). Sonic hedgehog acts at multiple stages during pancreatic tumorigenesis. Proc. Natl. Acad. Sci. USA *104*, 5103–5108.

Nolan-Stevaux, O., Lau, J., Truitt, M.L., Chu, G.C., Hebrok, M., Fernández-Zapico, M.E., and Hanahan, D. (2009). GLI1 is regulated through Smoothened-independent mechanisms in neoplastic pancreatic ducts and mediates PDAC cell survival and transformation. Genes Dev. *23*, 24–36.

Olive, K.P., Jacobetz, M.A., Davidson, C.J., Gopinathan, A., McIntyre, D., Honess, D., Madhu, B., Goldgraben, M.A., Caldwell, M.E., Allard, D., et al. (2009). Inhibition of Hedgehog signaling enhances delivery of chemotherapy in a mouse model of pancreatic cancer. Science *324*, 1457–1461.

Pasca di Magliano, M., Sekine, S., Ermilov, A., Ferris, J., Dlugosz, A.A., and Hebrok, M. (2006). Hedgehog/Ras interactions regulate early stages of pancreatic cancer. Genes Dev. *20*, 3161–3173.

Provenzano, P.P., Cuevas, C., Chang, A.E., Goel, V.K., Von Hoff, D.D., and Hingorani, S.R. (2012). Enzymatic targeting of the stroma ablates physical barriers to treatment of pancreatic ductal adenocarcinoma. Cancer Cell *21*, 418–429.

Rhim, A.D., Mirek, E.T., Aiello, N.M., Maitra, A., Bailey, J.M., McAllister, F., Reichert, M., Beatty, G.L., Rustgi, A.K., Vonderheide, R.H., et al. (2012). EMT and dissemination precede pancreatic tumor formation. Cell *148*, 349–361.

Roberts, D.J., Smith, D.M., Goff, D.J., and Tabin, C.J. (1998). Epithelial-mesenchymal signaling during the regionalization of the chick gut. Development *125*, 2791–2801.

Sastra, S.A., and Olive, K.P. (2013). Quantification of murine pancreatic tumors by high-resolution ultrasound. Methods Mol. Biol. *980*, 249–266.

Singh, A., Greninger, P., Rhodes, D., Koopman, L., Violette, S., Bardeesy, N., and Settleman, J. (2009). A gene expression signature associated with "K-Ras addiction" reveals regulators of EMT and tumor cell survival. Cancer Cell *15*, 489–500.

Singh, M., Lima, A., Molina, R., Hamilton, P., Clermont, A.C., Devasthali, V., Thompson, J.D., Cheng, J.H., Bou Reslan, H., Ho, C.C., et al. (2010). Assessing therapeutic responses in Kras mutant cancers using genetically engineered mouse models. Nat. Biotechnol. *28*, 585–593.

Stoker, M.G., Shearer, M., and O'Neill, C. (1966). Growth inhibition of polyoma-transformed cells by contact with static normal fibroblasts. J. Cell Sci. *1*, 297–310.

Sukegawa, A., Narita, T., Kameda, T., Saitoh, K., Nohno, T., Iba, H., Yasugi, S., and Fukuda, K. (2000). The concentric structure of the developing gut is regulated by Sonic hedgehog derived from endodermal epithelium. Development *127*, 1971–1980.

Thayer, S.P., di Magliano, M.P., Heiser, P.W., Nielsen, C.M., Roberts, D.J., Lauwers, G.Y., Qi, Y.P., Gysin, S., Fernández-del Castillo, C., Yajnik, V., et al. (2003). Hedgehog is an early and late mediator of pancreatic cancer tumorigenesis. Nature *425*, 851–856.

Theunissen, J.W., and de Sauvage, F.J. (2009). Paracrine Hedgehog signaling in cancer. Cancer Res. *69*, 6007–6010.

Tian, H., Callahan, C.A., DuPree, K.J., Darbonne, W.C., Ahn, C.P., Scales, S.J., and de Sauvage, F.J. (2009). Hedgehog signaling is restricted to the stromal compartment during pancreatic carcinogenesis. Proc. Natl. Acad. Sci. USA *106*, 4254–4259.

Vonlaufen, A., Phillips, P.A., Xu, Z., Goldstein, D., Pirola, R.C., Wilson, J.S., and Apte, M.V. (2008). Pancreatic stellate cells and pancreatic cancer cells: An unholy alliance. Cancer Res. *68*, 7707–7710.

Walter, K., Omura, N., Hong, S.M., Griffith, M., Vincent, A., Borges, M., and Goggins, M. (2010). Overexpression of Smoothened activates the sonic hedgehog signaling pathway in pancreatic cancer-associated fibroblasts. Clin. Cancer Res. *16*, 1781–1789.

Watanabe, S., Ueda, Y., Akaboshi, S., Hino, Y., Sekita, Y., and Nakao, M. (2009). HMGA2 maintains oncogenic RAS-induced epithelial-mesenchymal transition in human pancreatic cancer cells. Am. J. Pathol. *174*, 854–868.

Xu, Z., Vonlaufen, A., Phillips, P.A., Fiala-Beer, E., Zhang, X., Yang, L., Biankin, A.V., Goldstein, D., Pirola, R.C., Wilson, J.S., and Apte, M.V. (2010). Role of pancreatic stellate cells in pancreatic cancer metastasis. Am. J. Pathol. *177*, 2585–2596.

Yonemasu, H., Takashima, M., Nishiyama, K.I., Ueki, T., Yao, T., Tanaka, M., and Tsuneyoshi, M. (2001). Phenotypical characteristics of undifferentiated carcinoma of the pancreas: A comparison with pancreatic ductal adenocarcinoma and relevance of E-cadherin, alpha catenin and beta catenin expression. Oncol. Rep. *8*, 745–752.